Hydrodynamics in Motile Active Matter

68

Roland G. Winkler and Gerhard Gompper

Contents

Abstract

Hydrodynamic interactions determine the individual and collective behavior of nano- to micrometer size active objects such as swimming bacteria, sperm, algae, and synthetic colloidal microswimmers. Based on the Navier-Stokes equations of hydrodynamics, the major contributions to the flow field of a swimmer in a

R. G. Winkler (✉) · G. Gompper
Institute for Advanced Simulation and Institute for Complex Systems, Forschungszentrum Jülich, Jülich, Germany
e-mail: r.winkler@fz-juelich.de; g.gompper@fz-juelich.de

W. Andreoni, S. Yip (eds.), *Handbook of Materials Modeling*,
https://doi.org/10.1007/978-3-319-44677-6_35

Newtonian fluid are presented. The propulsion of beating and rotating filaments is shown to emerge as consequence of the distinct friction coefficients for parallel and perpendicular motion of the filament. Hydrodynamic interactions with a wall lead to a preferred alignment of a swimmer adjacent to a wall. Moreover, the rotational motion of a flagellar bundle of swimming bacteria combined with the counterrotation of the cell body leads to circular trajectories on a surface, where the handedness depends on the wall slip. Even more, the collective behavior of active matter is determined by hydrodynamic interactions, which is illustrated by cilia synchronization and the squirmer model for microswimmers.

1 Introduction

Active matter, whose agents consume internal energy or extract energy from the environment to propel themselves through a fluid, and are thus far from thermal equilibrium, is omnipresent in nature. Examples on the microscale range from an uncountable number of bacteria in soil or living in symbiosis with humans, spermatozoa in their attempt to fertilize an ovum, or algae harvesting sunlight in ponds and the ocean. Nowadays, synthetic active systems have been designed, which are powered by phoretic processes, e.g., thermophoresis or diffusiophoresis (Bechinger et al. 2016). In any case, the microswimmer is embedded in a fluid, and the fluid plays a decisive role for the propulsion itself as well as the collective behavior (Lauga and Powers 2009; Yeomans et al. 2014; Elgeti et al. 2015; Zöttl and Stark 2016; Winkler 2016). The physics ruling swimming on the micrometer scale is very different from that applying to swimming in the macro-world, although certain propulsion strategies are reminiscent of those on a macro-scale – bacteria, such as *Escherichia coli*, are propelled by rotating flagella, sperm perform a snakelike motion, and algae, such as *Chlamydomonas reinhardtii*, apply a breaststroke-type beating pattern. However, swimming at the micrometer scale is swimming at low-Reynolds numbers (Purcell 1977), where viscous damping by far dominates over inertia. Hence, swimming concepts of the high-Reynolds number macro-world are ineffective on small scales. In the evolutionary process, microorganisms acquired propulsion strategies, which successfully overcome and even exploit viscous drag.

Bacteria, sperm, or algae use flagella – filamentous structures protruding from their bodies – for their propulsion (cf. Fig. 1 for an illustration). In fact, eukaryotic flagella are very different from prokaryotic ones, which is manifested in the differing propulsion strategies (Elgeti et al. 2015). However, in any case, the thrust force emerges by the difference in the hydrodynamic friction of a (long) slender body parallel and perpendicular to the body major axis. Thereby, the flow field far from the swimmer is usually dominated by a "force dipole" and decays similarly with distance, independent of the propulsion mechanism, since a microswimmer is force- and torque-free. At walls, surface hydrodynamic interactions lead to a propulsion-dependent preferred alignment of a microswimmer (Spagnolie and Lauga 2012) or circular trajectories (Lauga et al. 2006; Di Leonardo et al. 2011; Hu et al. 2015a). Under shear flow, the hydrodynamic force-dipole flow field substantially affects

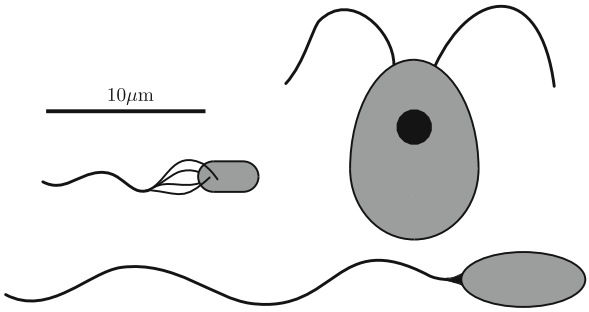

Fig. 1 Depiction of microswimmers. (Left) *E. Coli*, (Right) *Chlamydomonas* with the cell nucleus, and (Bottom) *sperm*. The scale bar indicates the approximate size of the swimmers

the overall viscosity (Saintillan 2010), and for suspensions of pushers, e.g., *E. coli* bacteria, "superfluidlike" behavior has been observed, where the viscous resistance to shear vanishes (López et al. 2015).

Active matter exhibits fascinating emergent collective phenomena. In nature, microswimmers can reach astonishing densities. Sperm cells are released by the millions to compete in the run for the egg, and biofilms are made up of billions of bacteria. Coordinated motion is exploited by spermatozoa of some species by self-assembling into unique train-like aggregates of hundreds or thousands of cells and thereby significantly increased sperm motility in a viscous environment (Sivinski 1984; Moore and Taggart 1995). Flagellated bacteria exhibit a particular mode of motion, where they migrate collectively over surfaces and are able to form stable aggregates, which can become highly motile (Heinrichsen 1978; Copeland and Weibel 2009; Kearns 2010). Here, cooperativity reaches a new level, and bacteria exhibit highly organized movements with remarkable large-scale patterns such as networks, complex vortices, or swarms (Copeland and Weibel 2009; Wensink et al. 2012). These type of patterns are remarkably similar to patterns appearing for other active matter systems such as schools of fish, flocks of birds, mammalian herds, or crowds of humans (Vicsek and Zafeiris 2012; Elgeti et al. 2015; Popkin 2016).

The various aspects touched above illustrate the fundamental importance of hydrodynamics for microscopic active matter ranging from swimming of individuals to large-scale collective migration. In the following, the low-Reynolds number aspects relevant for microswimmers will be briefly summarized, and various hydrodynamic phenomena will be presented.

2 Low-Reynolds Number Hydrodynamics

2.1 Equations of Motion

Typically, the dynamics of the (isothermal) incompressible fluid flow field surrounding a microswimmer is described by the Navier-Stokes equations

$$\rho\left(\frac{\partial}{\partial t}\boldsymbol{v}+(\boldsymbol{v}\cdot\nabla)\,\boldsymbol{v}\right)=-\nabla p+\eta\nabla^2\boldsymbol{v}+\boldsymbol{f}\,,\qquad \nabla\cdot\boldsymbol{v}=0, \tag{1}$$

where $\boldsymbol{v}(\boldsymbol{r},t)$, $p(\boldsymbol{r},t)$, and $\boldsymbol{f}(\boldsymbol{r},t)$ are the velocity, pressure, and volume-force density fields, respectively. At small Reynolds numbers $Re = \rho u L/\eta \ll 1$, where ρ is the fluid mass density, u the characteristic velocity, L the size of the microswimmer, and η the fluid viscosity, the inertia terms on the left-hand side of Eq. (1) can be neglected, and the equations reduce to the Stokes or creeping flow equations

$$\nabla p(\boldsymbol{r})-\eta\nabla^2\boldsymbol{v}(\boldsymbol{r})=\boldsymbol{f}(\boldsymbol{r})\,,\qquad \nabla\cdot\boldsymbol{v}=0. \tag{2}$$

For illustration, the Reynolds number in water of a swimmer of length $L = 10\,\mu$m, a velocity of $u = 50\mu$m/s, and the kinematic viscosity $\nu = \eta/\rho = 10^{-6}\text{m}^2/\text{s}$ is $Re \approx 10^{-3}$. The Stokes equation (2) is linear and time independent. The consequences of this intrinsic symmetry under time reversal for microswimmers undergoing periodic shape changes were first expressed by Purcell (1977) and are now known as "scallop theorem", which can be stated as: if the shape changes displayed by a swimmer are identical when viewed in reverse order (time reversal symmetry), it will generate an oscillatory, but no directed motion (Purcell 1977; Lauga and Powers 2009; Yeomans et al. 2014; Elgeti et al. 2015). Thus, just by opening and closing its two shells, a mussel (scallop) cannot move forward at $Re \ll 1$. Microswimmers developed various strategies to beat the scallop theorem. Aside from many (elastic) degrees of freedom, they use specific propulsion mechanisms which are not time reversible – bacteria such as *E. coli* are propelled by rotating helical flagella bundles, sperm use sinusoidal bending waves propagating from head to tail, and algae, e.g., *Chlamydomonas*, use a nonreciprocal stroke pattern.

2.2 Solution of Stokes Equation

The linear Stokes equations (2) are easily solved analytically for an unbounded fluid. The respective fluid velocity field is

$$\boldsymbol{v}(\boldsymbol{r})=\int\mathbf{Q}(\boldsymbol{r}-\boldsymbol{r}')\boldsymbol{f}(\boldsymbol{r}')\,d^3r'\,,\qquad Q_{\alpha\alpha'}(\boldsymbol{r})=\frac{1}{8\pi\eta r}\left[\delta_{\alpha\alpha'}+\frac{r_\alpha r_{\alpha'}}{r^2}\right], \tag{3}$$

where $\mathbf{Q}(\boldsymbol{r})$ is the well-known Oseen tensor, with the Cartesian components $Q_{\alpha\alpha'}$ ($\alpha,\alpha'\in\{x,y,z\}$) and $r = |\boldsymbol{r}|$ (Kim and Karrila 1991; Dhont 1996). The Oseen tensor, also denoted as Stokeslet, shows that hydrodynamic interactions are long ranged, with a $1/r$ decay like the Coulomb potential, and are anisotropic due to the incompressibility of the fluid. The Oseen tensor is the Green's function of the Stokes equation (2), which is evident, when the point force $\boldsymbol{f}(\boldsymbol{r}) = f_0\delta(\boldsymbol{r})\boldsymbol{e}$ in the direction $\boldsymbol{e}$ ($|\boldsymbol{e}| = 1$) is inserted. Then, Eq. (3) yields

$$\boldsymbol{v}(\boldsymbol{r}) = \frac{f_0}{8\pi\eta r}\left[\boldsymbol{e} + \frac{(\boldsymbol{r}\cdot\boldsymbol{e})\boldsymbol{r}}{r^2}\right]. \tag{4}$$

The magnitude of the flow field is twice larger in the force direction than perpendicular to it.

2.3 Microswimmer Flow Field

Most microswimmers move autonomously, with no external force or torque applied, and hence the total force/torque of the swimmer on the fluid and *vice versa* vanishes. In the simplest case, which actually applies to many microswimmers like bacteria, spermatozoa, or algae, the far-field hydrodynamics (at distances from the swimmer much larger than its size) can well be described by a force dipole (Lauga and Powers 2009; Ishikawa 2009). This has been confirmed experimentally for *E. coli* (Drescher et al. 2010, 2011) and in simulations (Hu et al. 2015b). The flow field of *Chlamydomonas* is well reproduced by three Stokeslets (Drescher et al. 2010).

Mathematically, the flow field $\boldsymbol{v}(\boldsymbol{r}-\boldsymbol{r}_0)$ of a hydrodynamic force dipole located at $\boldsymbol{r}_0$ follows by a superposition of two Stokeslets (4) with opposite forces $\boldsymbol{f}_0 = \pm f_0\boldsymbol{e}$ of equal magnitude at $\boldsymbol{r}_0 \pm \boldsymbol{l}/2$, where $\boldsymbol{l} = l\boldsymbol{e}$ and l is the distance between the Stokeslets. Taylor expansion to leading order in $|\boldsymbol{l}|/|\boldsymbol{r}-\boldsymbol{r}_0|$ yields

$$\boldsymbol{v}(\boldsymbol{r}) = \frac{P}{8\pi\eta}\boldsymbol{v}^{FD}(\boldsymbol{r})\,, \quad \boldsymbol{v}^{FD}(\boldsymbol{r}) = \frac{\boldsymbol{r}}{r^3}\left[-1 + 3\frac{(\boldsymbol{r}\cdot\boldsymbol{e})^2}{r^2}\right], \tag{5}$$

where $P = \pm f_0 l$ is the dipole strength. Note that the flow field of a force dipole decays as $1/r^2$ from the center of the dipole, faster than the force monopole or Stokeslet Eq. (3). The flow fields of hydrodynamic dipoles are shown in Fig. 2. In two dimensions, there are two inflow (left, right) and two outflow (top, bottom) regions, which are separated by the separatrices $z = \pm\sqrt{2}x$. In three dimensions, the outflow region is a cone.

Two classes of dipole swimmers can be distinguished. A swimmer with its "motor" in the back, and a passive body dragging along the surrounding fluid in front, creates a "pusher" flow field (cf. Fig. 2 (left)). Similarly, a swimmer with its "motor" in front, and the passive body dragging along the fluid behind, develops a "puller" flow field. This field follows by inversion of the arrows in Fig. 2 (left), i.e., the flow fields of pushers and pullers look similar but with opposite flow directions. This has important consequences for the interactions between swimmers and of swimmers with walls, as will be explained below.

The dipolar flow field and higher-order multipoles follow by a systematic expansion of the Oseen tensor in Eq. (3) (Kim and Karrila 1991; Pozrikidis 1992; Spagnolie and Lauga 2012). For a sphere of radius R, the swimmer far field up to order $\mathcal{O}(r^{-4})$ is dominated by the force dipole (FD) (Eq. (5)), source dipole (SD), force quadrupole (FQ), source quadrupole (SQ), and rotlet dipol (RD) contributions

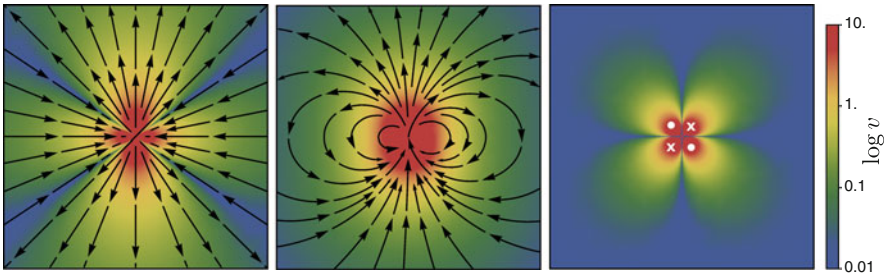

Fig. 2 (Left) Flow lines in the far-field of a hydrodynamic force dipole (5) and (Middle) a source dipole (7) oriented along the vertical direction. (Right) The flow field of the rotlet dipole (10) is rotational symmetric around the horizontal axis. The white crosses and bullets indicate the intersections of the flow lines with the plane

$$\begin{aligned}\boldsymbol{v}(\boldsymbol{r}) = \kappa^{FD}\boldsymbol{v}^{FD}(\boldsymbol{r}) + \kappa^{SD}\boldsymbol{v}^{SD}(\boldsymbol{r}) + \kappa^{FQ}\boldsymbol{v}^{FQ}(\boldsymbol{r}) + \kappa^{SQ}\boldsymbol{v}^{SQ}(\boldsymbol{r}) \\ + \kappa^{RD}\boldsymbol{v}^{RD}(\boldsymbol{r}) + \mathcal{O}(r^{-4}),\end{aligned} \tag{6}$$

where

$$\boldsymbol{v}^{SD}(\boldsymbol{r}) = -\frac{1}{r^3}\left(-\boldsymbol{e}_z + \frac{3z\boldsymbol{r}}{r^2}\right), \tag{7}$$

$$\boldsymbol{v}^{FQ}(\boldsymbol{r}) = \frac{1}{r^3}\left[\left(1 - \frac{3z^2}{r^2}\right)\boldsymbol{e}_z + \left(\frac{15z^3}{r^4} - 9\frac{z}{r^2}\right)\boldsymbol{r}\right], \tag{8}$$

$$\boldsymbol{v}^{SQ}(\boldsymbol{r}) = \frac{3}{r^4}\left(\frac{5z^2\boldsymbol{r}}{r^3} - \frac{2z\boldsymbol{e}_z + \boldsymbol{r}}{r}\right), \tag{9}$$

$$\boldsymbol{v}^{RD}(\boldsymbol{r}) = \frac{3z\boldsymbol{e}_z \times \boldsymbol{r}}{r^5}, \tag{10}$$

which decay like r^{-2}, r^{-3}, r^{-4}, and r^{-3}, respectively (Spagnolie and Lauga 2012). Note that in Eq. (7) the swimming direction $\boldsymbol{e}$ points along the positive z-axis, i.e., $\boldsymbol{e} \equiv \boldsymbol{e}_z$. The various factors κ account for the strength of the respective multipole, where $\kappa^{FD} = P/8\pi\eta$, $\kappa^{SD} = -v_0R^3/2$, and $\kappa^{SQ} = 3PR^3/8\pi\eta$.

Aside from the force-dipole term, most relevant for microswimmer are the source-dipole term $(1/r^3)$ due to the volume of the swimmer and the rotlet-dipole term $(1/r^3)$, e.g., for *E. coli* bacteria by the opposite rotation of the cell body and the flagella bundle.

3 Swimming Due to Flagellar Motion

3.1 Friction of Slender Body

Many microorganisms are propelled in a fluid by beating or rotating a flagellum. Thereby, a swimmer exploits the viscous frictional properties of the fluid environment, specifically, the anisotropic friction of a slender body. The frictional anisotropy can be demonstrated for a long and thin rod of radius R and length L. Considering the rod as composed of a sequence of beads with no-slip boundary conditions, the beat velocity is equal to the fluid velocity of Eq. (3). Under the influence of an external constant force $\boldsymbol{F} = F\boldsymbol{e}$, the average velocity of a rod aligned along the z-axis of the reference system is (Elgeti et al. 2015)

$$\boldsymbol{v}_{\text{rod}} = F\frac{\boldsymbol{e} + (\boldsymbol{e}_z \cdot \boldsymbol{e})\boldsymbol{e}_z}{4\pi\eta L^2}\int_{2R}^{L}\frac{L-s}{s}ds \tag{11}$$

in the limit of a continuous rod. The lower cutoff of the integral excludes a region of the thickness of the rod. Because $(\boldsymbol{e}_z \cdot \boldsymbol{e})\boldsymbol{e}_z$ is 1 and 0 for parallel and perpendicular orientation of the force with the rod axis, respectively, evaluation of the integral and the relation $\boldsymbol{F} = \zeta_\parallel \boldsymbol{v}_\parallel + \zeta_\perp \boldsymbol{v}_\perp$ yields

$$\zeta_\perp = 2\zeta_\parallel\,, \qquad \zeta_\perp = \frac{4\pi\eta L}{\ln(L/2R)} \tag{12}$$

in the asymptotic limit of a long rod. Hence, pulling a rod along its axis is easier than perpendicular to it. The logarithmic divergence is a result of the long-range nature of hydrodynamic interactions between different parts of the rod. Thus, hydrodynamic interactions reduce the friction coefficient compared to that of a rod of hydrodynamically noninteracting beads, where $\zeta_\perp = \zeta_\parallel \sim L$. Corrections of the friction coefficients for a more precise account of hydrodynamics for a cylinder have been calculated (Tirado et al. 1984).

3.2 Propulsion by Beating Flagella

The time-dependent shape of a sinusoidally beating flagellum with a planer beat (xz-plane) $z(x,t)$ and its local velocity $v_z(x,t)$ at the position x along its contour are described by

$$z(x,t) = A\sin(kx - wt), \quad v_z(x,t) = \frac{\partial z}{\partial t} = -A\omega\cos(kx - \omega t), \tag{13}$$

where A is the amplitude, ω the frequency, and k the wave number. Decomposing the velocity $\boldsymbol{v}(x,t) = (0, 0, v_z(x,t))^T$ into a component parallel $\boldsymbol{v}_\parallel = (\boldsymbol{v}\cdot\boldsymbol{t})\boldsymbol{t}$ and perpendicular $\boldsymbol{v}_\perp = \boldsymbol{v} - \boldsymbol{v}_\parallel$ to the local tangent vector $\boldsymbol{t} \sim (1, 0, Ak\cos(kx - \omega t))^T$ yields

$$\boldsymbol{v}_{\parallel} = -\frac{A^2 \omega k \cos^2(kx - \omega t)}{1 + A^2 k^2 \cos^2(kx - \omega t)}\, \boldsymbol{t}. \tag{14}$$

The separation $\boldsymbol{F} = \zeta_{\parallel} \boldsymbol{v}_{\parallel} + \zeta_{\perp} \boldsymbol{v}_{\perp}$ gives the average force of the flagellum in the swimming direction

$$F_z = (\zeta_{\parallel} - \zeta_{\perp}) \frac{1}{L} \int \frac{A^2 \omega k \cos^2(kx - \omega t)}{1 + A^2 k^2 \cos^2(kx - \omega t)}\, dx, \tag{15}$$

while the average force in the perpendicular direction vanishes. For small beating amplitudes, Eq. (15) can easily be integrated, which yields the average propulsion force

$$F_z = \frac{1}{2} (\zeta_{\parallel} - \zeta_{\perp}) A^2 \omega k, \tag{16}$$

and the swimming velocity, $v_{\text{flag}} \approx F_z / \zeta_{\parallel}$, (Gray and Hancock 1955)

$$v_{\text{flag}} = -\frac{1}{2} \left(\frac{\zeta_{\perp}}{\zeta_{\parallel}} - 1 \right) A^2 \omega k \, . \tag{17}$$

This simplified calculation shows several important aspects of flagellar propulsion. First, swimming is only possible due to the frictional anisotropy, i.e., $\zeta_{\parallel} \neq \zeta_{\perp}$. Second, for a traveling wave in the positive x-direction, the flagellum moves in the negative x-direction, i.e., movement is opposite to the direction of the traveling wave. Third, the swimming velocity increases linearly with the beating frequency ω and the wave vector k but quadratically with the beating amplitude A. And finally, the swimming velocity is independent of the fluid viscosity for a given beating amplitude.

3.3 Propulsion by Helical Flagella

Propulsion by rotation of helical flagella can also be illustrated by resistive force theory. Rotation of a rodlike segment in the direction $\boldsymbol{v}'$, where $v' = |\boldsymbol{v}'| = R_h \Omega$ (cf. Fig. 3), with R_h the helix radius and Ω its rotation frequency, yields the thrust force contribution F_T and the torque M_z (Lauga and Powers 2009)

$$F_T = (\zeta_{\parallel} - \zeta_{\perp}) v' \cos\vartheta \sin\vartheta \approx (\zeta_{\parallel} - \zeta_{\perp}) \vartheta R_h \Omega, \quad M_z = \zeta_{\perp} R_h v' = \zeta_{\perp} R_h^2 \Omega, \tag{18}$$

where $\vartheta \ll 1$ is assumed. Hence, the relation between force, torque, and translational and rotational velocity is

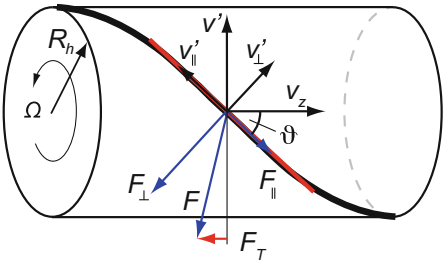

Fig. 3 Helical segment moving in a viscous fluid. Only half of a helical pitch is shown. The drag-based thrust force F_T appears by the rotation of the red rodlike segment in the direction $\boldsymbol{v}'$. The orientation angle ϑ is related with the pitch angle by $\pi/2 - \vartheta$. (From Elgeti et al. 2015)

$$\begin{pmatrix} F_z \\ M_z \end{pmatrix} = \begin{pmatrix} \zeta_\parallel & -(\zeta_\perp - \zeta_\parallel)\vartheta R_h \\ -(\zeta_\perp - \zeta_\parallel)\vartheta R_h & \zeta_\perp R_h^2 \end{pmatrix} \begin{pmatrix} v_z \\ \Omega \end{pmatrix}, \tag{19}$$

with $F_z = \zeta_\parallel v_z$ in case of no helix rotation. For a spherical cell body of radius R_b and with the assumption $R_b \ll L$, the frictional body force F_b and the body torque M_b are

$$F_b = \zeta_b v_z, \quad M_b = -\zeta_r^b \omega_b, \tag{20}$$

where $\zeta_b = 6\pi\eta R_b$ and $\zeta_r^b = 8\pi\eta R_b^3$ are the translation and rotational friction coefficients. The helix is driven by a rotary motor with the frequency Ω_m relative to the body. In response, the helix and body rotate with the frequencies Ω and Ω_b. These frequencies are related by $\Omega + \Omega_b = \Omega_m$. Since the whole bacterium is force- and torque-free, i.e., $F_z + F_b = 0$ and $M_z + M_b = 0$, its swimming velocity is obtained as

$$v_z \approx \vartheta \left(\frac{\zeta_\perp}{\zeta_\parallel} - 1 \right) \frac{\zeta_r^b}{\zeta_\perp R_h} \Omega_m. \tag{21}$$

The friction coefficient ζ_b does not appear, since $\zeta_\parallel \gg \zeta_b$ ($L \gg R_b$) is assumed. Evidently, swimming is again – as in the sperm case – only possible due to frictional anisotropy. Moreover, v_z depends linearly on the body rotational friction coefficient. Hence, without body, the bacterium could not swim. Due to the approximation $\vartheta \ll 1$, v_z depends linearly on the orientation angle ϑ. Changing the handedness of the helix leads to a change of the swimming direction.

Note that a helix driven by an external torque also moves forward; however, it is not torque-free, and therefore is not an autonomous swimmer.

3.4 Bacteria Swimming

A wide variety of bacteria exploits the propulsion strategy described in Sect. 3.3. Different species possess various numbers and differing arrangements of flagella. According to the arrangement, flagellated bacteria are classified as monotrichous bacteria with a single flagellum only, lophotrichous bacteria with multiple flagella located at a particular spot on their surface, amphitrichous bacteria with a single flagellum on each of the two opposite ends, and peritrichous bacteria which are covered by multiple flagella pointing in all directions. Prominent examples of peritrichous bacteria are *E. coli*, *Salmonella typhimurium*, *Rhizobium lupini*, or *Proteus mirabilis*, to name just a few. A flagellum is rotated by a motor complex, which consists of several proteins, and is anchored in the bacterial cell wall (Berg 2003). Bacteria like *E. coli* swim in a "run-and- tumble" motion (Berg 2003). In the "run" phase, the helical flagella are left-handed, and they rotate counterclockwise. The flagella form a bundle, and the bacterium moves forward in a direction determined by its long axis. At the beginning of the "tumble" phase, a flagellum rotational direction is reverted to clockwise. The flagellum leaves the bundle, which implies a random reorientation of the bacterium. The reversal of the rotational direction is accompanied by a change of the helical handedness from left-handed to right-handed, and the flagellum undergoes a polymorphic transition, i.e., assumes a different pitch and radius (Calladine 1975; Macnab 1977). At the end of the tumbling phase, all flagella start to rotate again in the same counterclockwise direction, the bundle reforms, and the bacterium returns to a directional motion. The flagella of bacteria like *Rhizobium meliloti* or *Rhizobium lupini* are only capable of limited polymorphic transitions, and their motors are unidirectional (Platzer et al. 1997). These bacteria modulate the rotation speed of individual motors to induce tumbling.

Since bacterial cells are force- and torque-free, the rotational motion of the flagellum bundle leads to a counterrotation of the cell body, i.e., swimming bacteria possess a rotlet dipole (cf. Eq. (10)). This has consequences for their hydrodynamic interactions, specifically with surfaces and interfaces.

The flow field of an *E. coli* bacterium obtained from experiment and simulations is presented in Fig. 4. In both cases, the far field is well described by the force-dipole field of Eq. (5) (Drescher et al. 2011; Hu et al. 2015b).

4 Surface Interaction

4.1 Dipole Swimmer Near a Wall: Swimming with an Image

The swimming behavior of microorganisms is typically altered by the presence of nearby obstacles or boundaries. In fact, most bacteria in nature live on surfaces, e.g., in biofilms (Copeland and Weibel 2009; Spagnolie and Lauga 2012). Correspondingly, attraction of such microorganisms to surfaces is of major importance

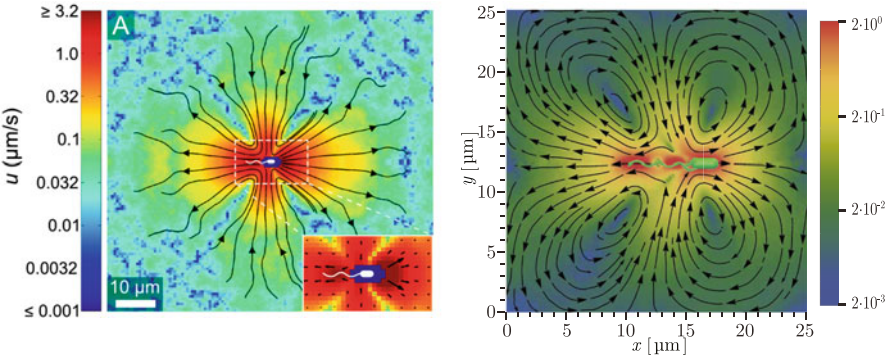

Fig. 4 Flow field of *E. coli* bacteria from (left) experiment (Drescher et al. 2011) and (right) simulations (Hu et al. 2015b). In simulations, a system with periodic boundary conditions is considered, which yields closed flow lines in contrast to the flow lines of the experimental bulk system. The logarithmic color scheme (right) indicates the magnitude of the flow speed scaled by the bacterial swimming velocity. (From Drescher et al. 2011 and Hu et al. 2015b)

and determines their microbial activity. Part of the attraction originates from hydrodynamic interactions of the swimmer with the surface. This is easily illustrated by a force dipole in front of a (slip) surface. The flow field of such a dipole can be obtained by the image method known from electrostatics. Considering, for simplicity, a planar wall with slip boundary conditions (cf. Fig. 5), at $z = 0$, the velocity field $v_{w,z}^{FD}$ perpendicular to the surface vanishes identically, i.e., $v_{w,z}^{FD}(z = 0) \equiv 0$. The flow field is then given by

$$\boldsymbol{v}_w^{FD}(\boldsymbol{r} - \boldsymbol{r}_0) = \boldsymbol{v}^{FD}(\boldsymbol{r} - \mathbf{r}_0; \boldsymbol{e}) + \boldsymbol{v}^{FD}(\mathbf{r} - \boldsymbol{r}_0'; \boldsymbol{e}'), \tag{22}$$

with $\boldsymbol{r}_0 = (x_0, y_0, z_0)$, $\boldsymbol{r}_0' = (x_0, y_0, -z_0)$, where $z_0 > 0$ and $\boldsymbol{e}'$ the mirror image of $\boldsymbol{e}$ with respect to the $z = 0$ plane. The dipole experiences a flow field and, hence, a force near the surface, which is determined by the hydrodynamic interactions between the dipole and its image. As a consequence, the dipole swimmer is moving toward the surface with the velocity

$$v_{w,z}^{FD}(z_0) = -\frac{P}{32\pi\eta z_0^2}\left[1 - 3(\boldsymbol{e} \cdot \boldsymbol{e}_z)^2\right], \tag{23}$$

because $(\boldsymbol{e}' \cdot \boldsymbol{e}_z)^2 = (\boldsymbol{e} \cdot \boldsymbol{e}_z)^2$. The result shows that the hydrodynamic force decays as a dipole flow field quadratic with the distance from the wall. The exact solution for a no-slip wall (Berke et al. 2008) yields the same functional dependence on the angle and the wall distance as Eq. (23), only the numerical prefactor in Eq. (23) is smaller by a factor 2/3.

The direction of the flow field depends on the dipole moment and its orientation. The hydrodynamic force is attractive to the wall for pusher ($P > 0$, sperm or

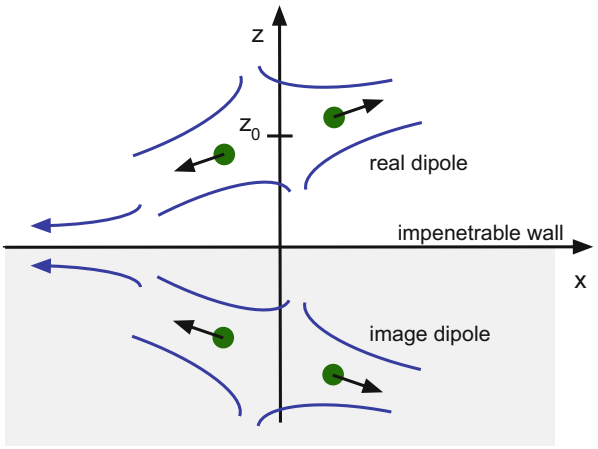

Fig. 5 Schematic representation of a dipole swimmer (pusher) near a wall. An image dipole ensures the correct boundary conditions at the impenetrable slip wall

bacteria) as long as $\cos\vartheta = (\boldsymbol{e}\cdot\boldsymbol{e}_z) < 1/\sqrt{3}$. Hence, pushers aligned parallel to the surface experience an attractive force. However, for pullers ($P < 0$, *Chlamydomonas*) hydrodynamic interactions are repulsive when they swim parallel to the wall, but they are attractive, when their orientation is nearly perpendicular to the wall. Yet, the average of the wall-induced interaction over a population of randomly oriented microorganisms is exactly equal to zero in a 3D system, since $\int v_{w,z}^{FD}(z_0)\sin\vartheta d\vartheta = 0$. As a consequence, the surface-induced velocity (23) alone cannot explain surface accumulation for initially randomly oriented incoming swimming cells.

The surface-induced hydrodynamic flow field is inhomogeneous and, thus, exerts a torque on the cell, which leads to a preferred alignment. The corresponding rotation rate is given by (Berke et al. 2008):

$$\Omega_r(\vartheta, z) = -\frac{3P\cos\vartheta\sin\vartheta}{64\pi\eta z^3}\left(1+\frac{\gamma^2-1}{2(\gamma^2+1)}(1+\cos^2\vartheta)\right), \tag{24}$$

where γ is the aspect ratio of the anisotropic swimmer. Since γ is typically larger than unity, the sign of Ω_r is determined by that of P and the product $\cos\vartheta\sin\vartheta$. When $0 \le \vartheta \le \pi/2$ or $\pi \le \vartheta \le 3\pi/2$, for a pusher the product is positive, and the rotation is negative, leading to parallel alignment with the surface. For the other angles, the rotation is positive, which leads to alignment too. Consequently, all pushers are oriented parallel to a surface and are attracted by the flow field. Pullers ($P < 0$) align normal to the surface. As both pushers and pullers come closer to the surface, higher orders in the multipole expansion become important (Spagnolie and Lauga 2012).

4.2 Bacteria Swimming at Surfaces

As a consequence of the rotlet dipole of bacteria by counterrotation of cell body and flagella bundle, hydrodynamic interactions lead to circular trajectories of bacteria at surfaces (Lauga et al. 2006; Di Leonardo et al. 2011; Hu et al. 2015a). Thereby, clockwise and counterclockwise trajectories appear, governed by the respective no-slip or slip boundary condition (cf. Fig. 6) (Lauga et al. 2006; Di Leonardo et al. 2011; Hu et al. 2015a; Elgeti et al. 2015; Elgeti and Gompper 2016). Moreover, the slip length determines the curvature of the circle. In qualitative agreement with experiments and quantitative agreement with theory and simulations, the trajectory curvature can well be described by

$$\kappa = \kappa_\infty + \frac{\kappa_0 - \kappa_\infty}{1 + b/h} \tag{25}$$

as function of the slip length b, where $\kappa_0 < 0$ and $\kappa_\infty > 0$ are the curvatures for the slip lengths $b = 0$ (no-slip) and $b = \infty$ (perfect slip), respectively, and h is an effective gap size between of the cell body and the surface (Hu et al. 2015a).

As found experimentally, the radius of the circle depends on the size of the cell body and increases linearly with body size. This fact can be exploited to separate cells of different sizes. As suggested by Hu et al. (2015a), a patterned surface with alternating hydrophobic and hydrophilic stripes leads to a preferred diffusion parallel to the stripes for radii on the order of the stripe widths, whereas for larger radii isotropic diffusion is obtained.

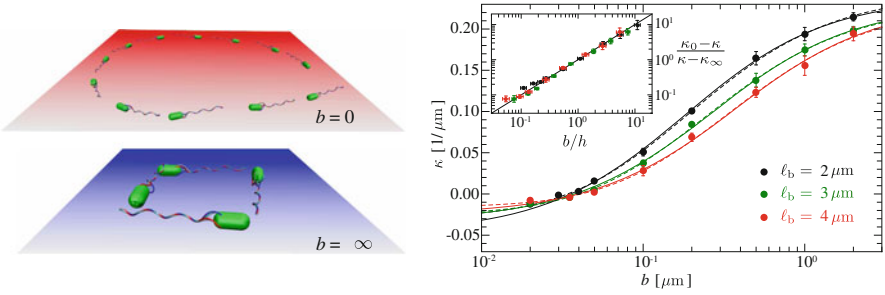

Fig. 6 (Left) Counterclockwise and clockwise circular trajectories from hydrodynamic simulations of an *E. coli*-type bacterium swimming near homogeneous surfaces with different slip lengths b as indicated. (Right) Effective curvatures of cells of various lengths, l_b, as function of the slip length. (From Hu et al. 2015a)

5 Squirmer: A Generic Model of Hydrodynamic Microswimmers

Generic models, which capture the essential swimming aspects, are crucial in theoretical studies of microswimmers. On the one hand, they help to unravel the relevant interaction mechanisms and, on the other hand, allow for the study of sufficiently large number of swimmers. A prominent example is the squirmer model (Lighthill 1952; Blake 1971). Originally, it was intended as a model for ciliated microswimmers, such as Paramecia. Nowadays, it is considered as a generic model for a broad class of microswimmers, ranging from diffusiophoretic particles to biological cells and has been applied to study collective effects in bulk, at surfaces, and in narrow slits (Ishikawa et al. 2006; Llopis and Pagonabarraga 2010; Zöttl and Stark 2014; Theers et al. 2016).

In its simplest form, a squirmer is represented as a spherical rigid colloid with a prescribed surface velocity. Restricting the surface velocity to be tangential, the slip velocity on the sphere surface can be expressed in terms of derivatives of Legendre polynomials, where the spherical squirmer is typically characterized by two modes only accounting for its swimming velocity (B_1) and its force dipole (B_2) (Ishikawa et al. 2006; Llopis and Pagonabarraga 2010). Explicitly, the leading contributions yield the slip velocity on the colloid surface (Ishikawa et al. 2006; Llopis and Pagonabarraga 2010; Theers et al. 2016)

$$\boldsymbol{v}_{sq} = (B_1 \sin\vartheta + B_2 \sin\vartheta\cos\vartheta)\boldsymbol{e}_\vartheta = B_1(\sin\vartheta + \beta\sin\vartheta\cos\vartheta)\boldsymbol{e}_\vartheta . \tag{26}$$

The parameter $B_1 = 2v_0/3$ is related to the swimming velocity, v_0, and $\beta = B_2/B_1$ accounts for the force dipole. The angle ϑ is measured with respect to the propulsion direction in a body-fixed reference frame. Higher-order terms can easily be taken into account (Elgeti et al. 2015; Llopis and Pagonabarraga 2010). The term with B_2 (or β) distinguishes various propulsion patterns, namely, pushers ($\beta < 0$), pullers ($\beta > 0$), and neutral squirmers ($\beta = 0$), corresponding, e.g., to *E. coli*, *Chlamydomonas*, or *Volvox*, respectively.

The far field of a squirmer is well described by the flow fields of a force dipole (FD), a source dipole (SD), and a source quadrupole (SQ)

$$\boldsymbol{v}(\boldsymbol{r}) = \kappa^{FD}\boldsymbol{v}^{FD}(\boldsymbol{r}) + \kappa^{SD}\boldsymbol{v}^{SD}(\boldsymbol{r}) + \kappa^{SQ}\boldsymbol{v}^{SQ}(\boldsymbol{r}) + \mathcal{O}(r^{-5}), \tag{27}$$

where the various terms are given in Eq. (5), (7), and (9).

The assumption of a spherical shape is adequate for swimmers like, e.g., *Volvox*; however, the shapes of other microswimmers (*E. coli, Chlamydomonas, Paramecium*) are nonspherical. Here, an extension of the squirmer concept to spheroidal objects has been proposed (Keller and Wu 1977; Theers et al. 2016). Figure 7 depicts flow fields of a spheroidal squirmer with the aspect ratio of two for the various kinds of dipolar terms in the laboratory and body-fixed reference frame. The near-field modifications by the finite-size swimmer is clearly visible in

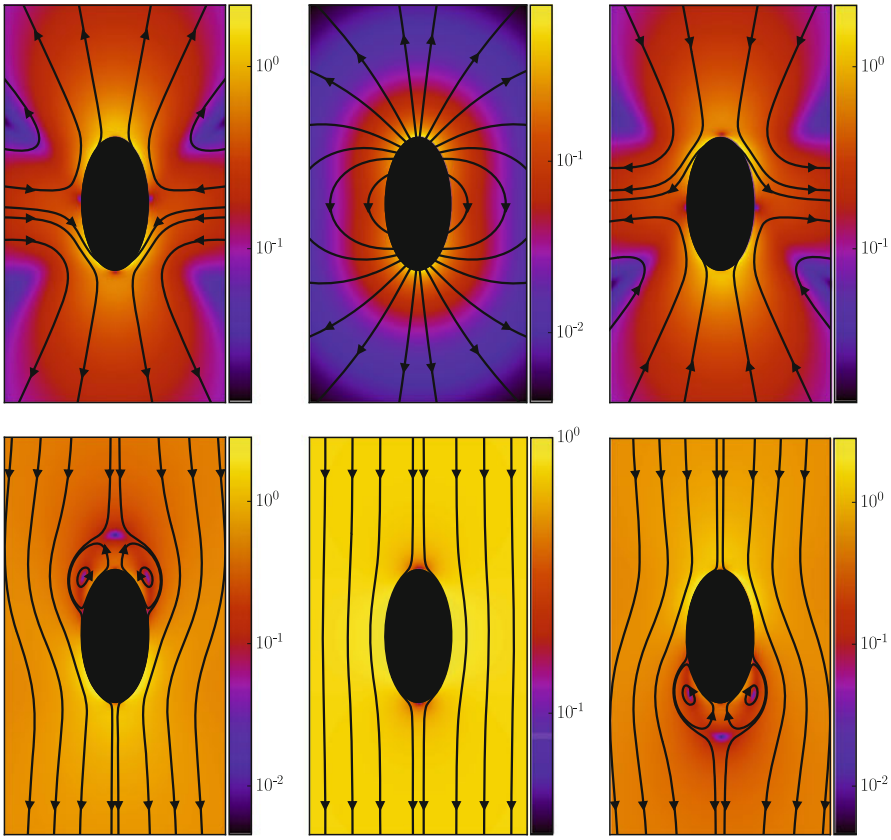

Fig. 7 Flow streamlines of isolated spheroidal squirmers. The top row corresponds to the laboratory reference frame and the bottom row to the body-fixed reference frame. (Left) Flow field of a pusher ($\beta = -3$), (Middle) a neutral squirmer $\beta = 0$, and (Right) a puller ($\beta = 3$). The magnitude of the relative velocity $3v/2v_0$ is color coded logarithmically. (The puller figures are from Theers et al. 2016)

comparison with Fig. 2. Moreover, pusher and puller exhibit a stagnation point in front or back, respectively, in the body-fixed reference frame for $|\beta| > 1$.

6 Collective Phenomena

Collective phenomena governed by hydrodynamic interactions appear on the level of flagella or cilia as well as on the scale of the microswimmers themselves. Examples on the flagella scale are the synchronization of flagella rotation in the formation of bacteria bundles (Reichert and Stark 2005; Qian et al. 2009; Reigh et al. 2012) or the development of metachronal waves in arrays of beating cilia (Sleigh 1962; Elgeti and Gompper 2013).

The importance of hydrodynamic interactions on the collective dynamics of microswimmers is most easily demonstrated for squirmers. On the one hand, the effect of the force dipole (pusher, puller, neutral squirmer) is captured, and, on the other hand, both far- and near-field hydrodynamics is taken into account, and their relative importance can be elucidated. In accordance with bacteria in biofilms, the collective behavior of squirmers is either studied by strictly two-dimensional motion with three-dimensional hydrodynamic interactions or by swimmers confined in a narrow slit with a respective limitation of hydrodynamic interactions by the surfaces. In the latter case, the boundary interactions play a major role (Theers et al. 2018).

6.1 Cilia Synchronization: Metachronal Waves

Propulsion of unicellular and multicellular organisms by cilia is omnipresent. Thereby, fluid is pumped across their surface by anchored motile cilia (flagella) (Sleigh 1962). Moreover, in higher organisms and humans, cilia are involved in moving mucus in the lungs (Afzelius 1976), the emergence of the embryonic left-right asymmetry (Cartwright et al. 2004), and intercellular communication (Wang et al. 2006). Already in the 1960s, Sleigh (1962) observed that arrays of cilia beat neither randomly nor synchronously but in a wave pattern called a metachronal wave (MCW). Several theoretical models have been proposed to shed light onto the metachronal coordination by hydrodynamic interactions. A model of coupled rotating spheres placed near a no-slip wall proves useful in clarifying the diverse types of MCWs observed in nature (Brumley et al. 2012).

Deeper insight into coordinated beating is gained by simulations of anchored semiflexible filaments with a nonreciprocal beat, where a "trigger" mechanism switches between the power and recovery stroke. Simulations of an array of 60×60 cilia in a 3D explicit fluid yield metachronal waves emerging autonomously, despite the presence of significant noise (Elgeti and Gompper 2013). The beat pattern of an individual cilium can react to the surrounding fluid flow, because the model only imposes time-dependent curvature forces and employs geometric thresholds for the switch between power and recovery stroke, and vice versa. Figure 8 displays the beating pattern of an individual filament with an asymmetric power and recovery stroke. The hydrodynamically induced metachronal waves are visible in Fig. 8 (right).

6.2 Aggregation of Squirmers

The interactions between microswimmers depend on their relative orientation. Thereby, interactions of pushers and pullers in equivalent positions and orientations are equal in magnitude but opposite in sign, because of the opposite sign of their dipole strength P. Since swimmers typically meet at different relative positions and orientations and due to the stochastic motion of many interacting objects, scattering of microswimmers occurs, and cooperative swimming is the exception rather than

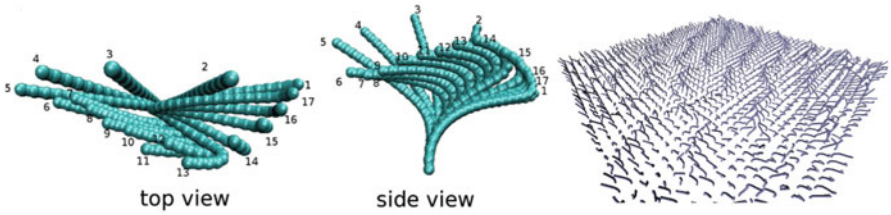

Fig. 8 (Left) Top and side view of the beat pattern of the computational cilia model. Subsequent conformations are equally spaced in time. The fast, planar power stroke (frames 1−5) continues until a positive curvature threshold in the lower part of the cilium is reached. The cilium then switches to a slow, out-of-plane recovery stroke (frames 6−17), which ends when a negative curvature threshold is exceeded. (Right) Simulation snapshot of an array of 40 × 40 beating cilia. Cilia are placed on a square lattice. The metachronal wave is easily recognized by the lines of fully extended cilia during the power stroke. (From Elgeti and Gompper 2013)

the rule in dilute suspensions (Ishikawa et al. 2006; Llopis and Pagonabarraga 2010; Götze and Gompper 2010). This applies to spherical as well as spheroidal squirmers. However, hydrodynamic interactions with confining surfaces in a slit geometry stabilize the cooperative swimming of spheroidal pulling squirmers, which emphasizes the relevance of hydrodynamic interactions in confinement (Theers et al. 2016).

Self-propelled particles exhibit a strong tendency for clustering and phase separation. The origin of this behavior is the blockage of motion when several particles collide with each other (cf. Fig. 9). The particular (small) cluster would dissolve after a time corresponding to the reorientation time of a swimmer. Interactions and collisions with other particles are controlled by the density and propulsion velocity v_0. Hence, if other particles collide before the original cluster dissolved, the cluster grows. This behavior already occurs for active Brownian particles (Bialké et al. 2012; Buttinoni et al. 2013; Redner et al. 2013; Palacci et al. 2013; Marchetti et al. 2016; Bechinger et al. 2016), i.e., for self-propelled particles with steric but without hydrodynamic interactions. The separation into a dense solid (2D) (Bialké et al. 2012; Marchetti et al. 2016; Bechinger et al. 2016) or fluid (3D) (Wysocki et al. 2014) phase and a dilute gas phase is denoted as motility-induced phase separation (MIPS) (Cates and Tailleur 2015). Hydrodynamic interactions strongly modify the collective behavior.

The collective swimming patterns of spherical squirmers in 2D exhibit a strong dependence on the sign of the force dipole (far field). Moreover, hydrodynamic near-field effects play an important role. The phase behavior of neutral squirmers ($\beta = 0$) with only far-field interactions is similar to that of active Brownian particles without hydrodynamic interactions (Yoshinaga and Liverpool 2017). The additional contribution due to hydrodynamics is an enhanced reorientation of the squirmers, which suppresses phase separation. Squirmer ensembles in 2D without thermal motion exhibit clustering for pullers and pushers due to near-field hydrodynamic interactions. Neutral squirmers spontaneously develop polar order and collectively

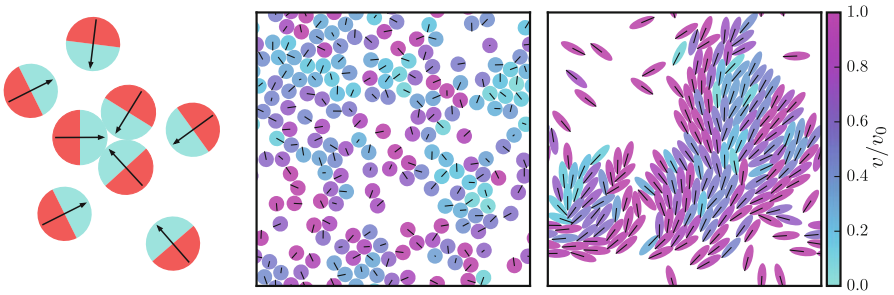

Fig. 9 (Left) Aggregation and cluster formation of squirmers by blockage. (Middle) Fluid phase of spherical squirmers and (Right) cluster of spheroidal squirmers confined in a slit at the two-dimensional packing fraction $\phi^{2D} = 0.5$ and the Péclet number $Pe = 12$. The Péclet number is defined as $Pe = v_0/2b_z D_R^{\perp}$, where b_z is the longer spheroid semiaxis and $D_R^{\perp}$ the rotational diffusion coefficient around the minor axis

move in a preferred direction (Kyoya et al. 2015; Yoshinaga and Liverpool 2017). Yet polar order is destroyed by thermal fluctuations. With fluctuations, all spherical squirmers exhibit cluster formation, however, with distinct characteristics. Here, cluster formation is most pronounced for pullers (Alarcón et al. 2017).

The anisotropic shape of a spheroidal squirmer enhances cluster formation compared to spherical swimmers (cf. Fig. 9) (Ginelli et al. 2010; Abkenar et al. 2013). This applies to ABPs as well as hydrodynamically coupled swimmers. Thereby, hydrodynamic interactions suppress motility-induced phase separation for spheres, whereas for spheroids hydrodynamic interactions enhance cluster formation in a slit geometry (Theers et al. 2018).

7 Conclusions

Hydrodynamic interactions are essential for active matter, specifically biological microswimmers. They are not only fundamental for the propulsion of microswimmers but also determine their behavior next to surfaces as well as the emergent collective dynamics and structures. Hydrodynamic interactions imply a very rich dynamics, which depends on the detailed swimming mechanism. For a fundamental understanding of the fluid-mediated interactions, consideration of the dominant multipole terms might suffice. However, the detailed collective properties depend also on the actual near-field flow. Hence, the full flow field has to be taken into account for a quantitative understanding of the local features of microswimmer aggregates. As a general conclusion, hydrodynamic interactions have to be taken into account for a qualitative and quantitative understanding of the emerging properties of active matter.

References

Abkenar M, Marx K, Auth T, Gompper G (2013) Collective behavior of penetrable self-propelled rods in two dimensions. Phys Rev E 88:062314

Afzelius B (1976) A human syndrome caused by immotile cilia. Science 193:317

Alarcón F, Valeriani C, Pagonabarraga I (2017) Morphology of clusters of attractive dry and wet self-propelled spherical particle suspensions. Soft Matter 13:814

Bechinger C, Di Leonardo R, Löwen H, Reichhardt C, Volpe G, Volpe G (2016) Active particles in complex and crowded environments. Rev Mod Phys 88:045006

Berg HC (2003) The rotary motor of bacterial flagella. Annu Rev Biochem 72:19

Berke AP, Turner L, Berg HC, Lauga E (2008) Hydrodynamic attraction of swimming microorganisms by surfaces. Phys Rev Lett 101:038102

Bialké J, Speck T, Löwen H (2012) Crystallization in a dense suspension of self-propelled particles. Phys Rev Lett 108:168301

Blake JR (1971) A spherical envelope approach to ciliary propulsion. J Fluid Mech 46:199

Brumley DR, Polin M, Pedley TJ, Goldstein RE (2012) Hydrodynamic synchronization and metachronal waves on the surface of the colonial alga *Volvox carteri*. Phys Rev Lett 109:268102

Buttinoni I, Bialké J, Kümmel F, Löwen H, Bechinger C, Speck T (2013) Dynamical clustering and phase separation in suspensions of self-propelled colloidal particles. Phys Rev Lett 110:238301

Calladine CR (1975) Construction of bacterial flagella. Nature 255:121

Cartwright JHE, Piro O, Tuval I (2004) Fluid-dynamical basis of the embryonic development of left-right asymmetry in vertebrates. Proc Natl Acad Sci USA 101:7234

Cates ME, Tailleur J (2015) Motility-induced phase separation. Annu Rev Condens Matter Phys 6:219

Copeland MF, Weibel DB (2009) Bacterial swarming: a model system for studying dynamic self-assembly. Soft Matter 5:1174

Dhont JKG (1996) An introduction to dynamics of colloids. Elsevier, Amsterdam

Di Leonardo R, Dell'Arciprete D, Angelani L, Iebba V (2011) Swimming with an image. Phys Rev Lett 106:038101

Drescher K, Goldstein RE, Tuval I (2010) Fidelity of adaptive phototaxis. Proc Natl Acad Sci USA 107:11171

Drescher K, Dunkel J, Cisneros LH, Ganguly S, Goldstein RE (2011) Fluid dynamics and noise in bacterial cell-cell and cell-surface scattering. Proc Natl Acad Sci USA 10940:108

Elgeti J, Gompper G (2013) Emergence of metachronal waves in cilia arrays. Proc Natl Acad Sci USA 110:4470

Elgeti J, Gompper G (2016) Microswimmers near surfaces. Eur Phys J Spec Top 225:2333

Elgeti J, Winkler RG, Gompper G (2015) Physics of microswimmers—single particle motion and collective behavior: a review. Rep Prog Phys 78:056601

Ginelli F, Peruani F, Bär M, Chaté H (2010) Large-scale collective properties of self-propelled rods. Phys Rev Lett 104:184502

Götze IO, Gompper G (2010) Mesoscale simulations of hydrodynamic squirmer interactions. Phys Rev E 82:041921

Gray J, Hancock GJ (1955) The propulsion of sea-urchin spermatozoa. J Exp Biol 32:802

Heinrichsen J (1978) Bacterial surface translocation: a survey and a classification. Bacteriol Rev 36:478

Hu J, Wysocki A, Winkler RG, Gompper G (2015a) Physical sensing of surface properties by microswimmers – directing bacterial motion via wall slip. Sci Rep 5:9586

Hu J, Yang M, Gompper G, Winkler RG (2015b) Modelling the mechanics and hydrodynamics of swimming *E. coli*. Soft Matter 11:7843

Ishikawa T (2009) Suspension biomechanics of swimming microbes. J R Soc Interface 6:815

Ishikawa T, Simmonds MP, Pedley TJ (2006) Hydrodynamic interaction of two swimming model micro-organisms. J Fluid Mech 568:119

Kearns DB (2010) A field guide to bacterial swarming motility. Nat Rev Microbiol 8:634

Keller SR, Wu TY (1977) A porous prolate-spheroidal model for ciliated micro-organisms. J Fluid Mech 80:259
Kim S, Karrila SJ (1991) Microhydrodynamics: principles and selected applications. Butterworth-Heinemann, Boston
Kyoya K, Matsunaga D, Imai Y, Omori T, Ishikawa T (2015) Shape matters: near-field fluid mechanics dominate the collective motions of ellipsoidal squirmers. Phys Rev E 92:063027
Lauga E, Powers TR (2009) The hydrodynamics of swimming microorganisms. Rep Prog Phys 72:096601
Lauga E, DiLuzio WR, Whitesides GM, Stone HA (2006) Swimming in circles: motion of bacteria near solid boundaries. Biophys J 90:400
Lighthill MJ (1952) On the squirming motion of nearly spherical deformable bodies through liquids at very small Reynolds numbers. Comm Pure Appl Math 5:109
Llopis I, Pagonabarraga I (2010) Hydrodynamic interactions in squirmer motion: swimming with a neighbour and close to a wall. J Non-Newtonian Fluid Mech 165:946
López HM, Gachelin J, Douarche C, Auradou H, Clément E (2015) Turning bacteria suspensions into superfluids. Phys Rev Lett 115:028301
Macnab RM (1977) Bacterial flagella rotating in bundles: a study in helical geometry. Proc Natl Acad Sci USA 74:221
Marchetti MC, Fily Y, Henkes S, Patch A, Yllanes D (2016) Minimal model of active colloids highlights the role of mechanical interactions in controlling the emergent behavior of active matter. Curr Opin Colloid Interface Sci 21:34
Moore HDM, Taggart DA (1995) Sperm pairing in the opossum increases the efficiency of sperm movement in a viscous environment. Biol Reprod 52:947
Palacci J, Sacanna S, Steinberg AP, Pine DJ, Chaikin PM (2013) Living crystals of light-activated colloidal surfers. Science 339:936
Platzer J, Sterr W, Hausmann M, Schmitt R (1997) Three genes of a motility operon and their role in flagellar rotary speed variation in *Rhizobium meliloti*. J Bacteriol 179:6391
Popkin G (2016) The physics of life. Nature 529:16
Pozrikidis C (1992) Boundary integral and singularity methods for linearized viscous flow. Cambridge University Press, Cambridge
Purcell EM (1977) Life at low Reynolds number. Am J Phys 45:3
Qian B, Jiang H, Gagnon DA, Breuer KS, Powers TR (2009) Minimal model for synchronization induced by hydrodynamic interactions. Phys Rev E 80:061919
Redner GS, Hagan MF, Baskaran A (2013) Structure and dynamics of a phase-separating active colloidal fluid. Phys Rev Lett 110:055701
Reichert M, Stark H (2005) Synchronization of rotating helices by hydrodynamic interactions. Eur Phys J E 17:493
Reigh SY, Winkler RG, Gompper G (2012) Synchronization and bundling of anchored bacterial flagella. Soft Matter 8:4363
Saintillan D (2010) The dilute rheology of swimming suspensions: a simple kinetic model. Exp Mech 50:1275
Sivinski J (1984) Sperm in competition. In: Smith RL (ed) Sperm competition and the evolution of animal mating systems. Academic, Orlando, p 174
Sleigh MA (1962) The Biology of Cilia and Flagella. Pergamon Press, Oxford
Spagnolie SE, Lauga E (2012) Hydrodynamics of self-propulsion near a boundary: predictions and accuracy of far-field approximations. J Fluid Mech 700:105
Theers M, Westphal E, Gompper G, Winkler RG (2016) Modeling a spheroidal microswimmer and cooperative swimming in a narrow slit. Soft Matter 12:7372
Theers M, Westphal E, Qi K, Winkler RG, Gompper G (2018) Clustering of microswimmers: interplay of shape and hydrodynamics. Soft Matter 14:8590–8603
Tirado MM, Martínez CL, de la Torre JG (1984) Comparison of theories for the translational and rotational diffusion coefficients of rod-like macromolecules. Application to short DNA fragments. J Chem Phys 81:2047
Vicsek T, Zafeiris A (2012) Collective motion. Phys Rep 517:71

Wang Q, Pan J, Snell WJ (2006) Intraflagellar transport particles participate directly in cilium-generated signaling in *Chlamydomonas*. Cell 125:549
Wensink HH, Dunkel J, Heidenreich S, Drescher K, Goldstein RE, Löwen H, Yeomans JM (2012) Meso-scale turbulence in living fluids. Proc Natl Acad Sci USA 109:14308
Winkler RG (2016) Low Reynolds number hydrodynamics and mesoscale simulations. Eur Phys J Spec Top 225:2079
Wysocki A, Winkler RG, Gompper G (2014) Cooperative motion of active Brownian spheres in three-dimensional dense suspensions. EPL 105:48004
Yeomans JM, Pushkin DO, Shum H (2014) An introduction to the hydrodynamics of swimming microorganisms. Eur Phys J Spec Top 223:1771
Yoshinaga N, Liverpool TB (2017) Hydrodynamic interactions in dense active suspensions: from polar order to dynamical clusters. Phys Rev E 96:020603
Zöttl A, Stark H (2014) Hydrodynamics determines collective motion and phase behavior of active colloids in quasi-two-dimensional confinement. Phys Rev Lett 112:118101
Zöttl A, Stark H (2016) Emergent behavior in active colloids. J Phys Condens Matter 28:253